Dyes and Pigments 92 (2012) 1250–1256

Contents lists available at SciVerse ScienceDirect

Dyes and Pigments

journal homepage: www.elsevier.com/locate/dyepig

Organic dyes with oligo-*n*-hexylthiophene for dye-sensitized solar cells: Relation between chemical structure of donor and photovoltaic performance

Shingo Kajiyama[a,b], Yu Uemura[a,c], Hidetoshi Miura[b], Kohjiro Hara[c], Nagatoshi Koumura[a,c,*]

[a] Graduate School of Pure and Applied Science, University of Tsukuba, Tsukuba, Ibaraki 305-8571, Japan
[b] Chemicrea Inc., 2-1-6 Sengen, Tsukuba, Ibaraki 305-0047, Japan
[c] National Institute of Advanced Industrial Science and Technology, Research Center for Photovoltaic Technology, 1-1-1 Higashi, Central 5, Tsukuba, Ibaraki 305-8565, Japan

ARTICLE INFO

Article history:
Received 9 June 2011
Received in revised form
23 August 2011
Accepted 24 August 2011
Available online 1 September 2011

Keywords:
Dye-sensitized solar cells
Organic dyes
Oligo-*n*-hexylthiophene linkage
Donor structures
Electron lifetime
Adsorption amount of dye

ABSTRACT

Organic dyes with the oligohexylthiophene linkage having several donor parts, carbazole, indole, and indoline, were newly synthesized as sensitizers for dye-sensitized solar cells. The carbazole was most efficient donor moiety for DSSCs among these dyes with the oligothiophene linkage. Carbazole dyes were adsorbed with larger amount of molecules on the TiO_2 film than both indole dyes and indoline dyes. Therefore, both the V_{OC} and the electron lifetime of DSSCs with the carbazole dyes were highly observed. The decreasing of J_{SC} of DSSCs with indole and indoline dyes also caused by the reducing the adsorption amount of dyes.

1. Introduction

Dye-sensitized solar cells (DSSCs) based on ruthenium complexes have attracted a great deal of interest since 1991 as they have the potential for low cost production and high efficiency [1]. Compared with ruthenium complexes [2–6] organic dyes, by virtue of their higher molar extinction coefficients and easier procedures for preparation and purification at low cost, are attracting more and more interest for application in DSSCs. Many kinds of organic dyes with anticipated power conversion efficiency (η) have been developed as sensitizers in DSSCs so far [7–26].

We have reported a series of dye molecules based on carbazole donor and alkyl-functionalized oligothiophenes as π-conjugation linkage for efficient DSSCs in our previous work (MK dyes) [27–31]. We proved that the existence of long alkyl chains on the oligothiophene linkage of the dye molecule can increase the electron lifetime and the open-circuit voltage by suppressing the aggregation of the dyes and electron recombination. However, the DSSCs based on MK dyes exhibited the relatively low short-circuit current density compared with other efficient organic dyes because of weak light harvesting ability in the long wavelength region (650–750 nm) due to the weak donor ability of carbazole. The absorption maxima of MK dyes, which are observed around 480 nm in 20%THF–toluene, were shown in shorter wavelength than those of organic dyes with a relatively strong donor of electron, such as coumarin (λ_{max} ~ 510 nm) [7], indoline (λ_{max} ~ 550 nm) [9] based dyes. Molecular design of dyes having long wavelength of absorption maxima will be necessary for improving light harvesting efficiency at longer wavelength up to 800 nm, and consequently solar-cell performance. To obtain organic dyes with the long wavelength of absorption maxima and the blocking effect caused by alkyl chains, new series of organic dyes with a strong donor and an oligoalkylthiophene linkage were designed. In this study, we have newly synthesized nine organic dyes (**MK-75**, **79**–**86**) based on three kinds of donor part (carbazole, indole, and indoline moiety) and cyanoacrylic acid acceptor part connected by a bi-3-*n*-hexylthiophene linkage, and investigated the photovoltaic performances of the DSSCs based on these dyes, described in Fig. 1. Until now no systematic studies have been done to search the donor moiety suitable for the oligothiophene linkage. Therefore, we first tried to find the relation between the donor ability of these dyes and their photovoltaic performances of DSSCs based on these dyes.

* Corresponding author. National Institute of Advanced Industrial Science and Technology, Research Center for Photovoltaic Technology, 1-1-1 Higashi, Central 5, Tsukuba, Ibaraki 305-8565, Japan. Tel.: +81 (0) 29 861 9322; fax: +81 (0) 29 861 6232.
E-mail address: n-koumura@aist.go.jp (N. Koumura).

0143-7208/$ – see front matter © 2011 Elsevier Ltd. All rights reserved.
doi:10.1016/j.dyepig.2011.08.016

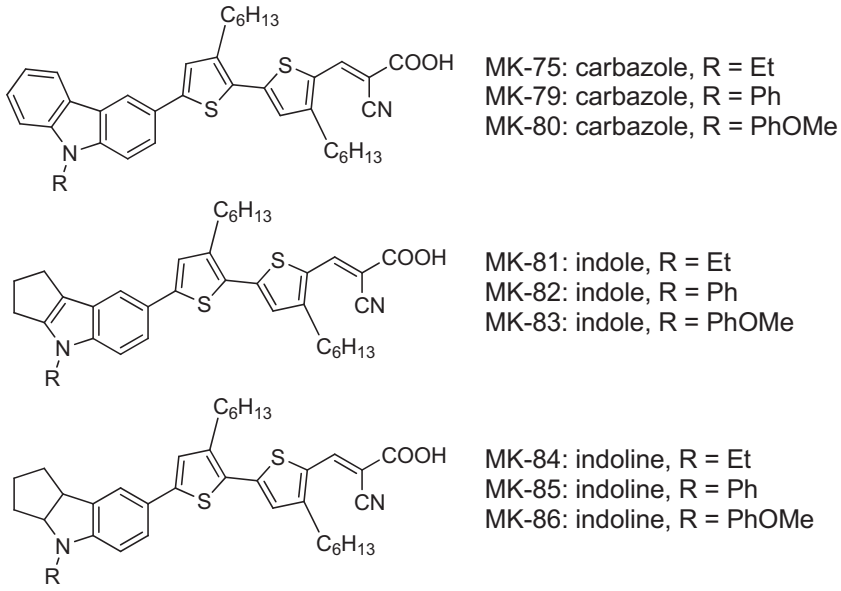

Fig. 1. Molecular structures of oligohexylthiophene based organic dyes for DSSCs.

Although the light harvesting ability of a dye was decreased around 650–750 nm area, a bi-3-*n*-hexylthiophene moiety was selected as the linkage because of facile syntheses of these dyes.

2. Results and discussion

Syntheses of dyes having a carbazole donor were accomplished by repeated bromination and Suzuki–Miyaura coupling reactions, Vilsmeier formylation, and Knoevenagel condensation starting from an *N*-substituted bromocarbazole as depicted in the previous report [27,31]. A 3-bromoindole donor, which was a starting compound, was constructed by Fischer-indole-synthesis method. After an introduction of a first *n*-hexylthiophene by Suzuki–Miyaura coupling into 3-bromoindole, a second thiophene was introduced by Mori's method [32] using a 5-iodo-3-*n*-hexylthiophene-2-carbaldehyde precursor because of unsuccessful bromination of the thiophene ring by *N*-bromosuccinimide. *N*-arylindoline dyes were synthesized by repeated bromination and Suzuki–Miyaura coupling, formylation by *n*-BuLi and *N*-formylpiperidine, and Knoevenagel reaction. The *N*-ethylindoline based dye was synthesized through the similar scheme of indole based dyes. The detailed experiments for the syntheses of these dyes are described in Supplementary data.

Table 1 summarized the results of absorption properties of these dyes in 20%THF–toluene solution. All dyes exhibit the moderate molar absorption coefficients (ε, ~39,000) as well as reported MK dyes regardless of the donor structure. Absorption maxima (λ_{max}) of dyes were varied: indoline (~509 nm) > indole = carbazole (~474 nm), which could be explained by the strength of electron donor ability of dyes.

Table 1
Absorption properties of dyes.[a]

Dye	Donor	R	λ_{max}/nm	ε/M^{-1} cm^{-1}
MK-75	Carbazole	Et	474	35,900
MK-79	Carbazole	Ph	473	38,900
MK-80	Carbazole	MeOPh	472	33,900
MK-81	Indole	Et	472	28,200
MK-82	Indole	Ph	471	35,600
MK-83	Indole	MeOPh	474	39,100
MK-84	Indoline	Et	513	31,800
MK-85	Indoline	Ph	498	34,000
MK-86	Indoline	MeOPh	509	34,100

[a] UV spectrum of each dye was measured in 20%THF–toluene solution through a 1 mm cell, respectively.

Fig. 2 shows the action spectra of incident photon-to-current conversion efficiency (IPCE) for DSSCs with these dyes, which was categorized by the substitution at the *N*-position of donor parts; (a) *N*-ethyl carbazole **MK-75**, indole **MK-81**, and indoline **MK-84**, (b) *N*-phenyl carbazole **MK-79**, indole **MK-82**, indoline **MK-85**, (c) *N*-anisyl carbazole **MK-80**, indole **MK-83**, indoline **MK-86**. The onset wavelength of IPCE spectra for DSSCs based on the indoline dyes, **MK-84**, **-85**, and **-86** were shifted to the longer wavelength (~40 nm) than those for the carbazole and indole dyes, suggesting the increased donor ability of the indoline moiety. The IPCE values more than 70% were observed in the range of 400–550 nm for the DSSC based on all carbazole dyes **MK-75**, **-79**, and **-80**, while the maximum values of IPCE for indole dyes **MK-81**, **-82**, and **-83** were slightly decreased. On the other hand, the IPCE values of DSSCs based on the indoline dyes, **MK-84**, **-85**, and **-86** were drastically decreased. These results indicated the shorter electron lifetime in TiO_2 of DSSCs with indoline dyes than those of carbazole dyes or the slower reduction rate of the indoline dye-cations from I^- in the electrolyte than those of the carbazole dye-cations. The IPCE spectra of DSSCs with each carbazole dye, which are depicted in Fig. 2(d), were similarly observed. The slightly long wavelength shift of the onset of the IPCE for **MK-75** was caused by the slightly stronger donor ability of the ethyl group on the nitrogen atom than those of *N*-aryl-substituted carbazole parts.

The photovoltaic performances of DSSCs employing these dyes under one sun conditions with thin-film TiO_2 electrodes (around 6 μm) are summarized in Table 2. As expected from the IPCE results, both of J_{SC} and V_{OC} for the DSSCs based on carbazole dyes were much higher than those for DSSCs based on indole and indoline dyes. Over 5% of the photon-to-current conversion efficiencies of DSSCs based on carbazole dyes were recorded under one sun conditions. Among the carbazole dyes, the J_{SC} values were influenced by the strength of the electron donation of *N*-substituent, Et (**MK-75**) > Ph (**MK-79**) ≈ MeOPh (**MK-80**), corresponding with the IPCE results. The decreasing of V_{OC} values of DSSCs based on the indole and indoline dyes compared with those of DSSCs with the carbazole dyes could be caused by the increasing the charge

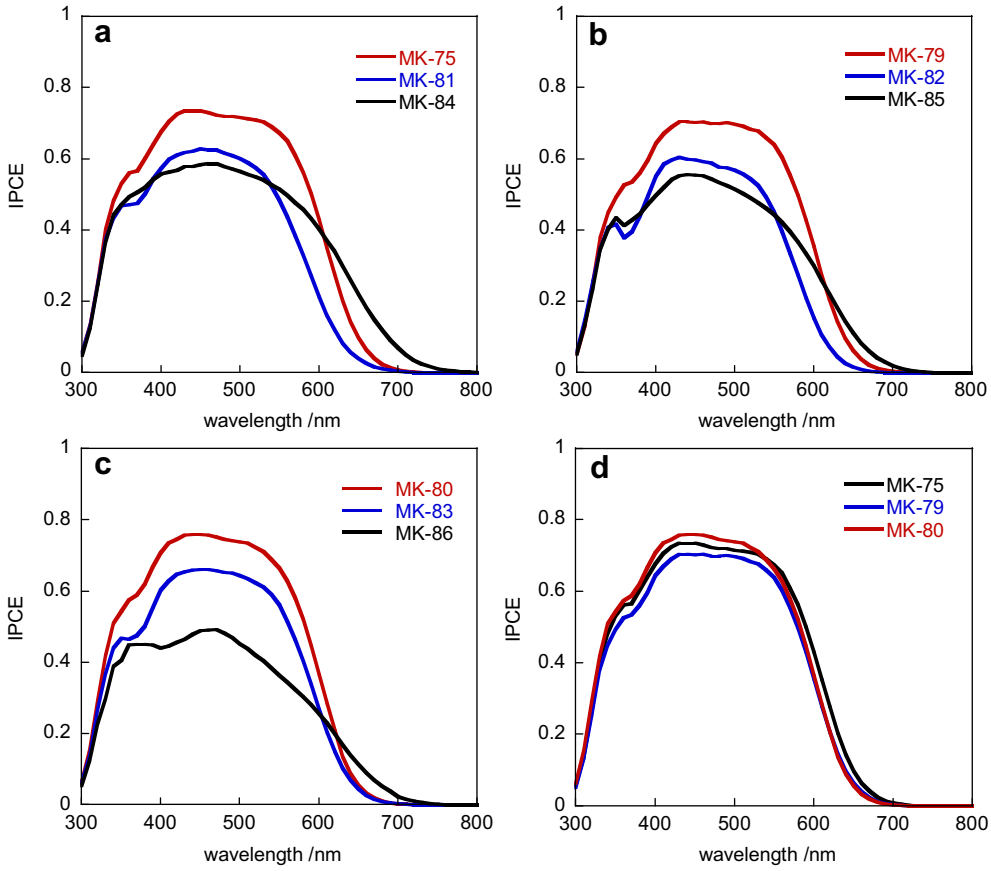

Fig. 2. IPCE spectra of DSSCs with dyes of *N*-anisyl substituted carbazole (red), indole (blue), and indoline (black) donor parts (a) for **MK-75**, **-81** and **-84**, (b) for **MK-79**, **-82**, and **-85**, (c) for **MK-80**, **-83**, and **-86**. (d) IPCE spectra of DSSCs with carbazole dyes, **MK-75**, **-79**, and **-80**. (For interpretation of the references to color in this figure legend, the reader is referred to the web version of this article.)

recombination from TiO_2 to dye-cations and/or I_3^-. The difference of the V_{OC} values is simply explained by the difference of the electron lifetimes in the DSSCs (Fig. 3(a)), because the potential difference between the conduction band edge of TiO_2 (E_{CB}) and I^-/I_3^- (E_{redox}), was not changed by these dyes (Fig. 3(b)). The electron lifetimes in DSSCs based on the indole and indoline dyes were lower than those in the DSSCs with the carbazole dyes. Especially, the electron lifetime in the DSSC/**MK-84** was observed to be lowest among these dyes. The trend of the electron lifetimes was corresponded with the results of the adsorption amount of dye molecules (Table 3 and Fig. 3(a)). In both case of indole and indoline dyes, the blocking effect by the hexyl-chains could be insufficient to suppress the recombination of electron in the TiO_2 electrode to the electrolyte because of the small amount of the adsorbed dyes. In other words, the physical blocking by the alkyl chains on the oligothiophene linkage to retard the approaching I_3^- to the TiO_2 surface is appeared to be effective when a large amount of dye molecules is adsorbed on the TiO_2 surface.

Table 2
Photovoltaic performances of DSSCs[a] and the adsorption amount of dyes on TiO_2 films.

Dye	ω[b]/μm	J_{SC}/mA cm^{-2}	V_{OC}/V	FF	η/%	Γ[c]/×10^{-4} mol cm^{-3}	$(J_{SC}/\omega)/\Gamma$[d]/×10^{8} mA mol^{-1}
MK-75	6.1	10.2	0.77	0.65	5.1	1.2	1.4
MK-79	5.9	9.71	0.76	0.72	5.3	1.3	1.3
MK-80	5.7	9.73	0.77	0.72	5.4	1.5	1.1
MK-81	6.1	7.63	0.64	0.72	3.5	0.73	1.7
MK-82	5.7	6.89	0.69	0.75	3.6	0.99	1.2
MK-83	6.0	8.00	0.67	0.72	3.9	0.93	1.4
MK-84	5.7	8.74	0.57	0.74	3.7	0.69	2.2
MK-85	5.9	7.82	0.65	0.66	3.4	0.89	1.5
MK-86	6.1	6.22	0.69	0.70	3.0	0.92	1.1

[a] Incident light: AM 1.5G (100 mW cm^{-2}) with a mask (0.2399 cm^2) and without an anti-reflection film. Electrolyte: 0.6 M DMPIml + 0.1 M LiI + 0.05 M I_2 + 0.5 M TBP in acetonitrile. TiO_2 electrode: film thickness around 6 μm.
[b] TiO_2 thickness.
[c] Γ is the adsorption amount of the dye on the TiO_2 film.
[d] J_{SC} values for a mole of adsorbed dye molecules.

The results of J_{SC} values for DSSCs with these dyes can be partially explained by the adsorption amount of the dyes on the TiO_2 film. The relatively low amount of dye-uptake on the TiO_2 nanoparticles originally caused the low photo-to-current conversion and the loss of electron in the TiO_2 electrode due to the charge recombination from TiO_2 to I_3^-. However, the differences of J_{SC} value was not exactly corresponded with the adsorption amount of dye molecules. According to the tentative J_{SC} values for a mole of dye-sensitizers ($(J_{SC}/\omega)/\Gamma$), shown in Table 2, the ethyl substituted indoline dye (**MK-84**) was most efficient for photo-to-current conversion, because the good absorption property at the long wavelength (~750 nm) was exhibited in the IPCE spectrum by the high donor ability. However, the energy conversion efficiency of the DSSC/**MK-84** was relatively low due to the highest charge recombination, which was discussed above.

The *I*–*V* curves in both light and dark conditions were described in Fig. 4(a)–(c), and all dark *I*–*V* curves are shown in Fig. 4(d). As the results that the similar trend of the dark *I*–*V* curves was obtained with that of the electron lifetimes under light conditions (Fig. 3(a)), the charge recombination pathway of the electron in TiO_2 could be mainly toward I_3^-, not dye-cations. However, for

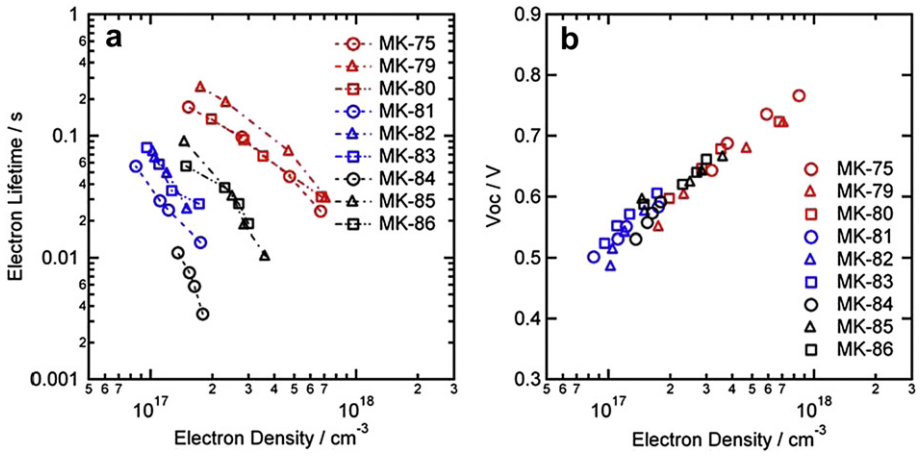

Fig. 3. (a) Electron lifetimes and (b) open-circuit voltage as a function of electron density in DSSCs.

indoline dyes **MK-85** and **-86** shown in Fig. 4(c), those dark and light *I*–*V* curves have cross points around the −0.2 mA cm^{-2}, respectively. This result suggested that the charge recombination from TiO_2 to dye-cations partially occurred. We also measured the cyclic voltammetry [33] of dye-loaded TiO_2 films and compared the HOMO–LUMO energy level of each dye on TiO_2 nanoparticles, depicted in Table 3. Note that the HOMO levels of the indoline dyes were more negative shifted than those of the carbazole and indole dyes. This result suggests a possibility of the slower reduction from I^- to the dye-cations of the indoline dyes compared with those of the other dyes because the HOMO levels of the indoline dyes are close to the potential of I^-/I_3^- (E_{redox}) [34,35]. In the case of the DSSC with **MK-84**, the charge recombination from TiO_2 to dye-cations could not be observed from the corresponded dark *I*–*V* curve (Fig. 4(c)) in spite of the negative shift of the HOMO energy level of a dye-loaded TiO_2 film. This result might be also explained by the low adsorption amount of dye molecules on a TiO_2 film.

3. Conclusions

To investigate the structural modification of dyes for DSSCs with the oligo-*n*-hexylthiophene linkage to enhance the absorption wavelength, we have synthesized the nine organic dyes having the bi-3-*n*-hexylthiophene unit, respectively, which have the different donor part, carbazole, indole, and indoline moieties. Although the indoline dyes with an oligothiophene linkage have potential properties for the light absorption at the long wavelength region as expected because of the higher donor ability than those for carbazole and indole dyes, the photo-to-current energy conversion efficiencies of DSSCs with indoline dyes were unfortunately worse than those for DSSC based on carbazole dyes due to decreasing the adsorption amount of dye molecules. Recently we have reported that the surface coverage on the TiO_2 electrode was very important for the achievement of efficient DSSCs by the changing of the alkyl-chain length on the oligothiophene linkage [36]. To obtain the efficient DSSCs with indoline dyes we have to improve the surface coverage on TiO_2 by increasing the adsorption amount of dye molecules or using a co-adsorbate. Additionally, the negative shift of HOMO energy levels of the indoline dyes close to the redox potential of electrolyte may cause the slow reduction of dye-cations from I^-. To obtain efficient DSSCs based on organic dyes with an oligothiophene linkage having an absorption property at the long wavelength region, the TiO_2 surface engineering with respect to the chemical structures of dye molecules should be particularly taken into consideration without harmful effects on the photovoltaic performances.

Table 3
Electrochemical properties of MK dyes.[a]

Dye	E_{HOMO} (V *vs.* NHE)	Gap (V)	E_{LUMO}[b] (V *vs.* NHE)
MK-75	0.92	1.94	−1.02
MK-79	0.97	2.09	−1.12
MK-80	1.08	2.08	−1.00
MK-81	1.12	2.07	−0.95
MK-82	1.01	2.07	−1.06
MK-83	0.95	2.10	−1.15
MK-84	0.66	1.92	−1.26
MK-85	0.75	1.92	−1.17
MK-86	0.67	1.88	−1.21

[a] The formal oxidation potential of the dyes were measured under the following conditions: dye-coated TiO_2 electrode (thickness: ca. 1.5 μm) as the working electrode, a Pt counter electrode, and a Ag/Ag^+ reference electrode (0.01 M $AgNO_3$ and 0.1 M tetrabutylammonium perchlorate in acetonitrile) in 0.1 M $LiClO_4$/acetonitrile. Potentials measured *vs.* Fc/Fc^+ were converted to NHE by addition of +0.63 V, which were taken as HOMO.

[b] The LUMO were calculated with the expression of LUMO = HOMO − gap, where the gap were derived from the absorption onset wavelength of the dye-loaded film.

4. Experimental

4.1. General procedure

Reagents and starting materials were purchased from Wako Chemicals, Kanto Chemicals, Tomiyama Pure Chemical Industries Ltd., Aldrich, Tokyo Chemical Industry Co., Ltd., and/or Merck and used without further purification. The solvents ware distilled and dried, if necessary, by standard methods. Column chromatography of all products was performed on silica gel (Kanto, Silica Gel 60N, spherical, 40–50 μm), and most of organic compounds were finally purified by the preparative HPLC (YRU-880 detector from SHIMAMURA Tec.) on silica gel (TOSOH, TSKgel Silica-60). The solvents ware distilled and dried, if necessary, by standard methods. ^1H NMR and ^{13}C NMR spectra were recorded on a Bruker Avance 400 (400 MHz). Chemical shifts were reported as δ values (ppm) relative to $CDCl_3$ or THF-d_8. The splitting patterns are designated as follows: s (singlet); d (doublet); t (triplet); q (quartet); m (multiplet) and br (broad). Absorption spectra were measured with a SHIMADZU UV-3101PC. The oxidation potential of the dye adsorbed on a TiO_2 film (thickness: ca. 1.5 μm) was measured by cyclic voltammetry using a dye-coated TiO_2 electrode as the working electrode, a Pt counter electrode, and a Ag/Ag^+ reference electrode (0.01 M $AgNO_3$ and 0.1 M tetrabutylammonium perchlorate in acetonitrile (AN)) in

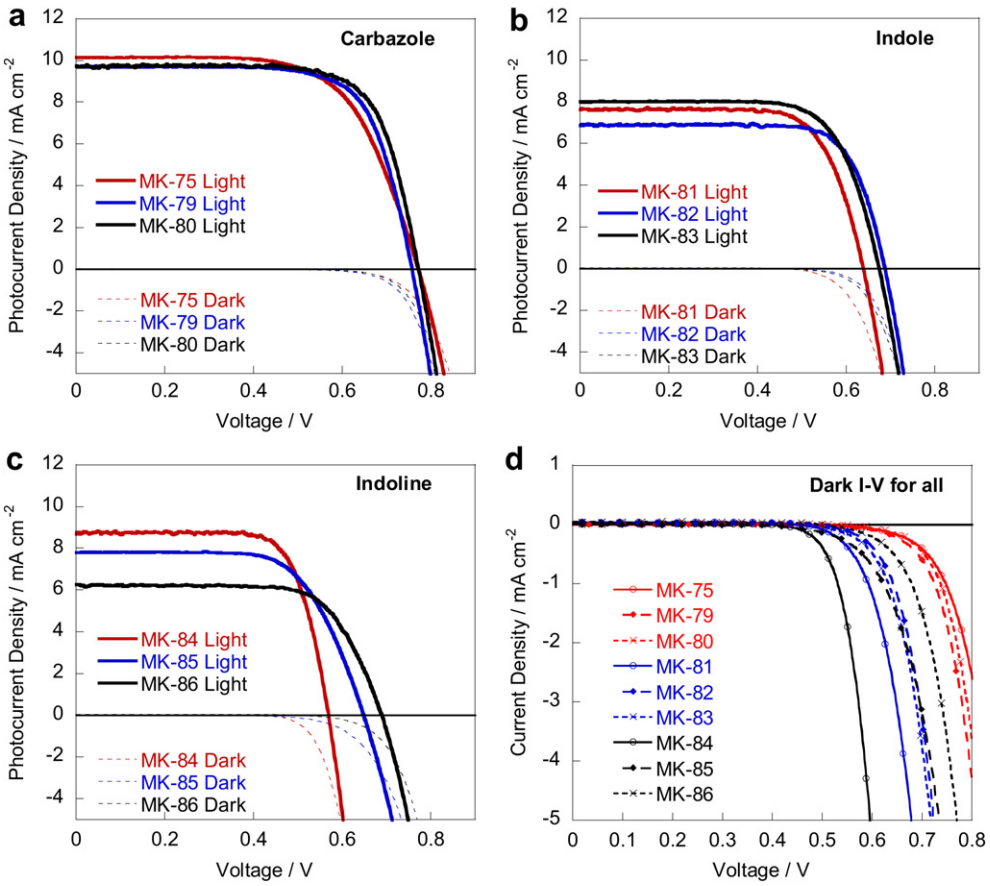

Fig. 4. *I–V* curves for DSSCs with nine dyes under the illumination of 100 mW cm^{-2} AM 1.5G simulated light and the dark condition. (a) carbazole dyes, (b) indole dyes, (c) indoline dyes, and (d) dark *I–V* curves for all.

0.1 M $LiCO_4$/AN. The measurements were performed with an electrochemical analyzer (HOKUTO DENKO, HZ-3000). The potential was calibrated against the ferrocene redox couple. Infrared spectra were measured with a PerkinElmer Spectrum One in ATR modes. MS (MALDI-TOF) analyses were measured by a Applied Biosystems Voyager-DE PRO. HRMS (ESI) analyses were measured by a API QSTAR Pulsar i.

4.2. Physical data of dyes

4.2.1. 2-Cyano-3-[5′-(9-ethyl-9H-carbazol-3-yl)-3′,4-di-n-hexyl-[2,2′]bithiophen-5-yl]acrylic acid, ***MK-75***

^{1}H NMR (400 MHz, THF-d_8) δ 8.41 (s, 1H), 8.16 (d, J = 7.6 Hz, 1H), 7.73 (d, J = 7.5 Hz, 1H), 7.49–7.42 (m, 3H), 7.35 (s, 1H), 7.22–7.19 (m, 2H), 4.40 (q, J = 5.5 Hz, 2H), 2.90 (t, J = 7.6 Hz, 2H), 2.82 (t, J = 7.6 Hz, 2H), 1.80–1.64 (m, 4H), 1.55–1.30 (m, 15H), 0.95–0.91 (m, 6H), ^{13}C NMR (100 MHz, THF-d_8) δ 165.0, 155.4, 146.9, 145.6, 144.5, 143.4, 141.5, 140.8, 130.1, 128.9, 128.7, 127.5, 126.8, 126.6, 125.5, 124.4, 124.4, 123.8, 121.3, 120.0, 118.2, 109.8, 109.7, 97.7, 38.2, 32.7, 32.6, 32.1, 31.4, 31.2, 30.3, 29.9, 29.5, 23.5, 23.5, 14.5, 14.5, 14.1, FT-IR ν_{max} (ATR) 2923, 2856, 2213, 1677, 1557, 1539, 1488, 1447, 1404, 1230, 1197 cm^{-1}, HRESIMS m/z 621.2597 $[M-H]^-$, Calcd for $C_{38}H_{42}N_2O_2S_2$: 621.2609.

4.2.2. 2-Cyano-3-[3′,4-di-n-hexyl-5′-(9-phenyl-9H-carbazol-3-yl)-[2,2′]bithiophen-5-yl]acrylic acid, ***MK-79***

^{1}H NMR (400 MHz, THF-d_8) δ 8.52 (s, 1H), 8.42 (s, 1H), 8.24 (d, J = 7.8 Hz, 1H), 7.74 (dd, J = 8.6, 1.7 Hz, 1H), 7.69–7.62 (m, 4H), 7.52 (t, J = 7.1 Hz, 1H), 7.44–7.39 (m, 4H), 7.31–7.27 (m, 2H), 2.95 (t, J = 8.0 Hz, 2H), 2.87 (t, J = 7.6 Hz, 2H), 1.83–1.67 (m, 4H), 1.58–1.51 (m, 2H), 1.45–1.36 (m, 10H), 0.95–0.91 (m, 6H), ^{13}C NMR (100 MHz, THF-d_8) δ 164.6, 155.5, 146.6, 145.6, 144.7, 143.5, 142.4, 141.7, 138.4, 130.9, 130.2, 128.9, 128.6, 127.9, 127.8, 127.2, 127.1, 126.8, 125.0, 124.8, 124.3, 121.3, 121.2, 118.3, 111.0, 110.7, 97.6, 32.7, 32.6, 32.2, 31.4, 31.2, 30.3, 29.9, 29.5, 23.53, 23.46, 14.5, 14.4, FT-IR ν_{max} (ATR) 2931, 2853, 2211, 1683, 1567, 1539, 1487, 1407, 1230, 1200 cm^{-1}, HRESIMS m/z 669.2585 $[M-H]^-$, Calcd for $C_{42}H_{42}N_2O_2S_2$: 669.2609.

4.2.3. 2-Cyano-3-{3′,4-di-n-hexyl-5′-[9-(4-methoxyphenyl)-9H-carbazol-3-yl]-[2,2′]bithiophen-5-yl}acrylic acid, ***MK-80***

^{1}H NMR (400 MHz, THF-d_8) δ 8.46 (s, 1H), 8.41 (s, 1H), 8.21 (d, J = 7.6 Hz, 1H), 7.67 (d, J = 7.2 Hz, 1H), 7.45 (d, J = 5.5 Hz, 2H), 7.40–7.36 (m, 2H), 7.30–7.24 (m, 3H), 7.19–7.15 (m, 3H), 3.88 (s, 3H), 2.89 (t, J = 7.7 Hz, 2H), 2.82 (t, J = 7.6 Hz, 2H), 1.80–1.64 (m, 4H), 1.57–1.50 (m, 2H), 1.41–1.35 (m, 10H), 0.95–0.91 (m, 6H), ^{13}C NMR (100 MHz, THF-d_8) δ 165.0, 160.3, 155.3, 146.5, 145.4, 144.5, 143.3, 142.8, 142.0, 130.7, 130.2, 129.2, 128.9, 127.5, 127.1, 126.8, 126.5, 124.6, 124.0, 121.2, 120.9, 118.1, 115.9, 110.8, 110.6, 97.9, 55.8, 32.7, 32.6, 32.1, 31.3, 31.2, 30.3, 29.9, 29.5, 23.6, 23.5, 14.52, 14.48, FT-IR ν_{max} (ATR) 2923, 2851, 2210, 1682, 1566, 1512, 1486, 1407, 1243 cm^{-1}, HRESIMS m/z 699.2735 $[M-H]^-$, Calcd for $C_{43}H_{44}N_2O_3S_2$: 699.2715.

4.2.4. 2-Cyano-3-[5′-(4-ethyl-1,2,3,4-tetrahydrocyclopenta[b]indol-7-yl)-3′,4-di-n-hexyl-[2,2′]bithiophen-5-yl] acrylic acid, ***MK-81***

^{1}H NMR (400 MHz, THF-d_8) δ 8.41 (s, 1H), 7.69 (s, 1H), 7.40 (d, J = 8.6 Hz, 1H), 7.32 (d, J = 8.6 Hz, 1H), 7.29 (s, 1H), 7.23 (s, 1H), 4.14 (q, J = 7.2 Hz, 2H), 2.94–2.84 (m, 8H), 2.59–2.52 (m, 2H), 1.81–1.67 (m, 4H), 1.57–1.50 (m, 2H), 1.43–1.35 (m, 13H), 0.95–0.91

(m, 6H), ^{13}C NMR (100 MHz, THF-d_8) δ 164.6, 155.6, 148.1, 147.7, 146.0, 144.6, 143.5, 141.7, 130.0, 128.2, 127.5, 126.3, 125.9, 125.3, 118.9, 118.8, 117.0, 116.6, 110.6, 97.3, 40.1, 32.7, 32.6, 32.2, 31.4, 31.7, 30.3, 29.9, 29.5, 29.2, 25.8, 25.6, 23.5, 23.5, 15.9, 14.5, 14.4, FT-IR ν_{max} (ATR) 2925, 2854, 2212, 1681, 1568, 1490, 1407, 1244, 1212 cm^{-1}, HRESIMS m/z 611.2741 [M − H]$^-$, Calcd for $C_{37}H_{44}N_2O_2S_2$: 611.2766.

4.2.5. 2-Cyano-3-[3′,4-di-n-hexyl-5′-(4-phenyl-1,2,3,4-tetrahydrocyclopenta[b]indol-7-yl)-[2,2′]bithiophen-5-yl]acrylic acid, **MK-82**

^{1}H NMR (400 MHz, THF-d_8) δ 8.41 (s, 1H), 7.77 (s, 1H), 7.57–7.50 (m, 4H), 7.42 (s, 2H), 7.39–7.34 (m, 2H), 7.25 (s, 1H), 2.95–2.91 (m, 6H), 2.87 (t, J = 7.6 Hz, 2H), 2.61–2.54 (m, 2H), 1.81–1.67 (m, 4H), 1.57–1.50 (m, 2H), 1.44–1.35 (m, 10H), 0.95–0.91 (m, 6H), ^{13}C NMR (100 MHz, THF-d_8) δ 164.6, 155.5, 147.7, 147.4, 145.8, 144.6, 143.5, 142.0, 139.7, 130.4, 130.1, 128.6, 127.7, 127.3, 126.7, 126.6, 125.5, 125.5, 121.5, 119.8, 117.0, 116.7, 111.9, 97.4, 32.7, 32.6, 32.2, 31.4, 31.2, 30.3, 29.9, 29.5, 29.1, 26.8, 25.8, 23.52, 23.46, 14.5, 14.4, FT-IR ν_{max} (ATR) 2922, 2853, 2212, 1683, 1566, 1491, 1407, 1237, 1089 cm^{-1}, HRESIMS m/z 659.2757 [M − H]$^-$, Calcd for $C_{41}H_{44}N_2O_2S_2$: 659.2766.

4.2.6. 2-Cyano-3-{3′,4-di-n-hexyl-5′-[4-(4-methoxyphenyl)-1,2,3,4-tetrahydrocyclopenta[b]indol-7-yl]-[2,2′]bithiophen-5-yl} acrylic acid, **MK-83**

^{1}H NMR (400 MHz, THF-d_8) δ 8.40 (s, 1H), 7.75 (s, 1H), 7.40–7.38 (m, 3H), 7.32–7.28 (m, 2H), 7.23 (s, 1H), 7.09 (d, J = 8.6 Hz, 2H), 3.86 (s, 3H), 2.94–2.83 (m, 8H), 2.59–2.52 (m, 2H), 1.80–1.66 (m, 4H), 1.57–1.50 (m, 2H), 1.44–1.35 (m, 10H), 0.94–0.92 (m, 6H), ^{13}C NMR (100 MHz, THF-d_8) δ 164.6, 159.6, 155.5, 148.0, 147.6, 145.9, 144.6, 143.5, 142.5, 132.3, 130.1, 128.5, 127.6, 127.1, 126.6, 126.4, 126.2, 120.7, 119.5, 117.0, 116.6, 115.5, 111.7, 97.3, 55.7, 32.7, 32.6, 32.2, 31.4, 31.2, 30.3, 29.9, 29.5, 29.1, 26.5, 25.6, 23.53, 23.46, 14.5, 14.4, FT-IR ν_{max} (ATR) 2926, 2853, 2211, 1682, 1567, 1512, 1489, 1407, 1241, 1033 cm^{-1}, HRESIMS m/z 689.2880 [M − H]$^-$, Calcd for $C_{42}H_{46}N_2O_3S_2$: 689.2872.

4.2.7. 2-Cyano-3-[5′-(4-ethyl-1,2,3,3a,4,8b-hexahydrocyclopenta[b]indol-7-yl)-3′,4-di-n-hexyl-[2,2′]bithiophen-5-yl]acrylic acid, **MK-84**

^{1}H NMR (400 MHz, THF-d_8) δ 8.40 (s, 1H), 7.31–7.29 (m, 2H), 7.17 (s, 1H), 7.10 (s, 1H), 6.30 (d, J = 8.4 Hz, 1H), 4.29 (t, J = 6.6 Hz, 1H), 3.73 (t, J = 7.9 Hz, 1H), 3.38–3.17 (m, 2H), 2.90–2.83 (m, 4H), 2.07–1.98 (m, 1H), 1.91–1.88 (m, 1H), 1.77–1.65 (m, 6H), 1.56–1.49 (m, 2H), 1.42–1.31 (m, 12H), 1.16 (t, J = 7.1 Hz, 3H), 0.94–0.91 (m, 6H), ^{13}C NMR (100 MHz, THF-d_8) δ 165.0, 155.4, 153.0, 147.6, 146.0, 144.6, 143.3, 135.3, 129.8, 127.1, 127.0, 126.5, 124.9, 122.8, 122.4, 117.1, 105.6, 97.3, 69.2, 46.5, 41.3, 40.6, 36.1, 34.2, 32.7, 32.6, 32.2, 31.3, 31.2, 30.2, 29.9, 29.5, 23.5, 23.5, 14.5, 14.4, 12.1, FT-IR ν_{max} (ATR) 2927, 2854, 2209, 1676, 1610, 1561, 1484, 1456, 1406, 1346, 1290, 1241, 1211 cm^{-1}, HRESIMS m/z 613.2935 [M − H]$^-$, Calcd for $C_{37}H_{46}N_2O_2S_2$: 613.2922.

4.2.8. 2-Cyano-3-[3′,4-di-n-hexyl-5′-(4-phenyl-1,2,3,3a,4,8b-hexahydrocyclopenta[b]indol-7-yl)-[2,2′]bithiophen-5-yl]acrylic acid, **MK-85**

^{1}H NMR (400 MHz, THF-d_8) δ 8.47 (s, 1H), 7.47 (s, 1H), 7.37–7.33 (m, 5H), 7.21 (d, J = 3.1 Hz, 2H), 7.00–6.96 (m, 2H), 4.91 (t, J = 6.6 Hz, 1H), 3.89 (t, J = 7.7 Hz, 1H), 2.92–2.84 (m, 4H), 2.17–2.06 (m, 1H), 1.95–1.84 (m, 3H), 1.79–1.66 (m, 6H), 1.58–1.31 (m, 12H), 0.95–0.91 (m, 6H), ^{13}C NMR (100 MHz, THF-d_8) δ 164.8, 155.5, 148.6, 146.6, 145.9, 144.6, 143.5, 143.4, 136.9, 130.0, 130.0, 127.8, 127.4, 125.9, 125.7, 125.2, 122.9, 122.6, 120.4, 117.1, 108.5, 97.3, 69.9, 46.2, 35.9, 34.5, 32.7, 32.6, 32.2, 31.3, 31.2, 30.3, 29.9, 29.5, 25.1, 23.5, 23.5, 14.5, 14.5, FT-IR ν_{max} (ATR) 2923, 2855, 2210, 1679, 1592, 1563, 1487, 1450, 1404, 1373, 1241, 1214 cm^{-1}, HRESIMS m/z 661.2931 [M − H]$^-$, Calcd for $C_{41}H_{46}N_2O_2S_2$: 661.2922.

4.2.9. 2-Cyano-3-{3′,4-di-n-hexyl-5′-[4-(4-methoxyphenyl)-1,2,3,3a,4,8b-hexahydrocyclopenta[b]indol-7-yl]-[2,2′]bithiophen-5-yl}acrylic acid, **MK-86**

^{1}H NMR (400 MHz, THF-d_8) δ 8.40 (s, 1H), 7.40 (s, 1H), 7.28 (dd, J = 8.3, 1.2 Hz, 1H), 7.22 (d, J = 9.0 Hz, 2H), 7.16 (s, 1H), 7.13 (s, 1H), 6.93 (d, J = 9.0 Hz, 2H), 6.64 (d, J = 8.4 Hz, 1H), 4.81 (t, J = 7.2 Hz, 1H), 3.82 (t, J = 9.0 Hz, 1H), 3.78 (s, 3H), 2.89–2.81 (m, 4H), 2.13–2.01 (m, 1H), 1.90–1.86 (m, 2H), 1.77–1.66 (m, 7H), 1.60–1.47 (m, 3H), 1.42–1.30 (m, 11H), 0.94–0.89 (m, 6H), ^{13}C NMR (100 MHz, THF-d_8) δ 165.0, 156.9, 155.4, 150.3, 146.9, 145.9, 144.6, 143.3, 136.5, 136.2, 129.9, 127.4, 127.2, 126.1, 125.3, 124.2, 123.9, 122.8, 117.2, 115.4, 107.3, 97.3, 70.7, 55.6, 46.3, 36.1, 34.3, 32.7, 32.6, 32.1, 31.3, 31.2, 30.3, 29.9, 29.5, 25.0, 23.5, 23.5, 14.5, 14.4, FT-IR ν_{max} (ATR) 2927, 2855, 2211, 1682, 1604, 1564, 1508, 1488, 1405, 1376, 1237, 1217 cm^{-1}, HRESIMS m/z 691.3050 [M − H]$^-$, Calcd for $C_{42}H_{48}N_2O_3S_2$: 691.3028.

4.3. Preparation of dye-sensitized TiO_2 electrodes

Nanocrystalline TiO_2 photoelectrodes were prepared by a screen printing technique. An organic TiO_2 paste for screen printing was purchased from SOLARONIX (T20/SP). The TiO_2 paste was printed on a glass substrate coated with transparent conducting oxide (TCO, F-doped SnO_2) and subsequently sintered at 500 °C in air for 1 h, and deposited aqueous $TiCl_4$, followed by heat treatment (450 °C, 30 min). The thickness of the TiO_2 thin films, measured with a Dektak 8 (Veeco), was ca. 6 μm. The MK dyes were dissolved at a concentration of 0.3 mM in toluene (KANTO CHEMICAL). The TiO_2 films were immersed in the dye solutions and then kept at 25 °C for more than 12 h to allow the dye to adsorb to the TiO_2 surface.

4.4. Adsorption amount of the dye on the TiO_2 film measurement

After the preparation of a dye-loaded TiO_2 film, the dye molecules were desorbed away from the TiO_2 electrode by immersing in the tetrabutylammonium hydroxide solution in 20%THF–toluene, and then UV–vis spectrum of the solution was measured. The adsorption amount of the dye (Γ) on the TiO_2 film was calculated from the absorbance of the solution and absorption coefficient (ε).

4.5. Photovoltaic measurements of the solar cells

The each photovoltaic cell, consisted of a dye-sensitized TiO_2 electrode, a Pt counter electrode sputtered (ca. 200 nm) onto TCO-coated glass plate, a film spacer (30 μm thickness) and an organic electrolyte, was prepared. The apparent surface area of the TiO_2 film electrode was ca. 0.25 cm^2. The electrolyte was 0.6 M 1,2-dimethyl-3-*n*-propylimidazolium iodide (DMPImI) + 0.1 M LiI + 0.05 M I_2 + 0.5 M 4-*tert*-butylpyridine (TBP) in AN. Reagent-grade LiI (WAKO CHEMICAL) and I_2 (WAKO) were used for the electrolyte. DMPImI was purchased from Tomiyama Pure Chemical Industries Ltd. The photovoltaic performance of the solar cells was measured with a source meter (ADVANTEST, R6243). We employed an AM 1.5G solar simulator (WACOM, WXS-80C-3 and YAMASHITA DENSO Co., YSS-150A) as the light source. The incident light intensity was calibrated by using a standard solar cell composed of a crystalline silicon solar cell and an IR-cut off filter (SCHOTT, KG-5), giving the photoresponse range of amorphous silicon solar cell (produced and calibrated by Japan Quality Assurance Organization). We used an aperture mask (0.2399 cm^2) attached onto the top of the cells in the photovoltaic measurements. Action spectra of the monochromatic incident photon-to-current conversion efficiency (IPCE) of the solar cell were measured with a CEP-99W system (BUNKOHKEIKI Co., Ltd.).

4.6. Electron lifetime measurements of DSSCs

Electron lifetimes (τ) were measured by stepped light-induced photocurrent and voltage transients (SLIM-PCV) method [37]. In short, DSSC was irradiated by a diode laser (635 nm, 10 mW, Lab-laser, Coherent), and less than 10% of the laser intensity was stepped down. The initial and final intensity were controlled by a PC through a D/A converter. Induced transients were measured by a fast multimeter having data storage (AD7461A, Advantest). The measurements were repeated under various laser intensities to measure light intensity-dependent τ. Electron densities (n) at open circuit were measured by a Charge Extraction Method [38]. In short, under laser irradiation, bias potential was applied to DSSC by a potentiostat (HA5001, Hokuto Denko) to have the condition equivalent to open circuit, and the current transients, induced by switching the intensity and bias potential to zero simultaneously, were measured. Measurements were repeated again under various light intensities to obtain the relationship between *V*oc and electron densities.

Acknowledgment

This work was partially supported by a Grant-in-Aid for Young Scientists (B) (No. 21750200) by Ministry of Education, Culture, Sports, Science and Technology (MEXT), Japan. The authors thank Prof. Kigoshi and Dr. Hayakawa to measure ESIMS spectra of dyes.

Appendix. Supplementary data

Supplementary data associated with this article can be found, in the online version, at doi:10.1016/j.dyepig.2011.08.016.

References

[1] O'Regan B, Grätzel M. A low-cost, high-efficiency solar cell based on dye-sensitized colloidal TiO_2 films. Nature 1991;353:737–40.
[2] Nazeeruddin MK, Kay A, Rodicio I, Humphry-Baker R, Mueller E, Liska P, et al. Conversion of light to electricity by cis-X2bis(2,2′-bipyridyl-4,4′-dicarboxylate)ruthenium(II) charge-transfer sensitizers (X = Cl−, Br−, I−, CN−, and SCN−) on nanocrystalline titanium dioxide electrodes. J Am Chem Soc 1993;115:6382–90.
[3] Nazeeruddin MK, Zakeeruddin SM, Humphry-Baker R, Jirousek M, Liska P, Vlachopoulos N, et al. Acid-base equilibria of (2,2′-bipyridyl-4,4′-dicarboxylic acid)ruthenium(II) complexes and the effect of protonation on charge-transfer sensitization of nanocrystalline titania. Inorg Chem 1999;38:6298–305.
[4] Wang P, Zakeeruddin SM, Exnar I, Grätzel M. High efficiency dye-sensitized nanocrystalline solar cells based on ionic liquid polymer gel electrolyte. Chem Commun; 2002:2972–3.
[5] Gao F, Wang Y, Shi D, Zhang J, Wang M, Jing X, et al. Enhance the optical absorptivity of nanocrystalline TiO_2 film with high molar extinction coefficient ruthenium sensitizers for high performance dye-sensitized solar cells. J Am Chem Soc 2008;130:10720–8.
[6] Chiba Y, Islam A, Watanabe Y, Komiya R, Koide N, Han L. Dye-sensitized solar cells with conversion efficiency of 11.1%. Jpn J Appl Phys 2006;45:L638–40.
[7] Hara K, Wang Z-S, Sato T, Furube A, Katoh R, Sugihara H, et al. Oligothiophene-containing coumarin dyes for efficient dye-sensitized solar cells. J Phys Chem B 2005;109:15476–82.
[8] Horiuchi T, Miura H, Sumioka K, Uchida S. High efficiency of dye-sensitized solar cells based on metal-free indoline dyes. J Am Chem Soc 2004;126:12218–9.
[9] Dentani T, Kubota Y, Funabiki K, Jin J, Yoshida T, Minoura H, et al. Novel thiophene-conjugated indoline dyes for zinc oxide solar cells. New J Chem 2009;33:93–101.
[10] Zhu W, Wu Y, Wang S, Li W, Li X, Chen J, et al. Organic D-A-π-A solar cell sensitizers with improved stability and spectral response. Adv Funct Mater 2011;21:756–63.
[11] Wu W, Yang J, Hua J, Tang J, Zhang L, Long Y, et al. Efficient and stable dye-sensitized solar cells based on phenothiazine sensitizers with thiophene units. J Mater Chem 2010;20:1772–9.
[12] Ko S, Choi H, Kang M-S, Hwang H, Ji H, Kim J, et al. Silole-spaced triarylamine derivatives as highly efficient organic sensitizers in dye-sensitized solar cells (DSSCs). J Mater Chem 2010;20:2391–9.
[13] Zhang G, Bala H, Cheng Y, Shi D, Lv X, Yu Q, et al. High efficiency and stable dye-sensitized solar cells with an organic chromophore featuring a binary π-conjugated spacer. Chem Commun; 2009:2198–200.
[14] Tang J, Wu W, Hua J, Li J, Li X, Tian H. Starburst triphenylamine-based cyanine dye for efficient quasi-solid-state dye-sensitized solar cells. Energy Environ Sci 2009;2:982–90.
[15] Tang J, Hua J, Wu W, Li J, Jin Z, Long Y, et al. New starburst sensitizer with carbazole antennas for efficient and stable dye-sensitized solar cells. Energy Environ Sci 2010;3:1736–45.
[16] Ooyama Y, Shimada Y, Inoue S, Nagano T, Fujikawa Y, Komaguchi K, et al. New molecular design of donor-π-acceptor dyes for dye-sensitized solar cells: control of molecular orientation and arrangement on TiO_2 surface. New J Chem 2011;35:111–8.
[17] Zeng W, Cao Y, Bai Y, Wang Y, Shi Y, Zhang M, et al. Efficient dye-sensitized solar cells with an organic photosensitizer featuring orderly conjugated ethylenedioxythiophene and dithienosilole blocks. Chem Mater 2010;22:1915–25.
[18] Lu M, Liang M, Han H-Y, Sun Z, Xue S. Organic dyes incorporating bis-hexapropyltruxeneamino moiety for efficient dye-sensitized solar cells. J Phys Chem C 2011;115:274–81.
[19] Hwang S, Lee JH, Park C, Lee H, Kim C, Park C, et al. A highly efficient organic sensitizer for dye-sensitized solar cells. Chem Commun; 2007:4887–9.
[20] Ning Z, Fu Y, Tian H. Improvement of dye-sensitized solar cells: what we know and what we need to know. Energy Environ Sci 2010;3:1170–81.
[21] Chen H, Huang H, Huang X, Clifford JN, Forneli A, Palomares E, et al. High molar extinction coefficient branchlike organic dyes containing di(p-tolyl) phenylamine donor for dye-sensitized solar cells applications. J Phys Chem C 2010;114:3280–6.
[22] Sayama K, Tsukagoshi S, Hara K, Ohga Y, Shinpou A, Abe Y, et al. Photoelectrochemical properties of J aggregates of benzothiazole merocyanine dyes on a nanostructured TiO_2 film. J Phys Chem B 2002;106:1363–71.
[23] Liang M, Lu M, Wang Q-L, Chen W-Y, Han H-Y, Sun Z, et al. Efficient dye-sensitized solar cells with triarylamine organic dyes featuring functionalized-truxene unit. J Power Sources 2011;196:1657–64.
[24] Burke A, Ito S, Snaith H, Bach U, Kwiatkowski J, Grätzel M. The function of a TiO_2 compact layer in dye-sensitized solar cells incorporating "planar" organic dyes. Nano Lett 2008;8:977–81.
[25] Yang X, Fang J-K, Suzuma Y, Xu F, Orita A, Otera J, et al. Synthesis and properties of 9,10-anthrylene-substituted phenyleneethynylene dyes for dye-sensitized solar cell. Chem Lett; 2011:620–2.
[26] Ning Z, Tian H. Triarylamine: a promising core unit for efficient photovoltaic materials. Chem Commun; 2009:5483–95.
[27] Koumura N, Wang Z-S, Mori S, Miyashita M, Suzuki E, Hara K. Alkyl-functionalized organic dyes for efficient molecular photovoltaics. J Am Chem Soc 2006;128:14256–7.
[28] Zhang X-H, Cui Y, Katoh R, Koumura N, Hara K. Organic dyes containing thieno[3,2-*b*]indole donor for efficient dye-sensitized solar cells. J Phys Chem C 2010;114:18283–90.
[29] Zhang X-H, Wang Z-S, Cui Y, Koumura N, Furube A, Hara K. Organic sensitizers based on hexylthiophene-functionalized indolo[3,2-*b*]carbazole for efficient dye-sensitized solar cells. J Phys Chem C 2009;113:13409–15.
[30] Koumura N, Wang Z-S, Miyashita M, Uemura Y, Sekiguchi H, Cui Y, et al. Substituted carbazole dyes for efficient molecular photovoltaics: long electron lifetime and high open circuit voltage performance. J Mater Chem 2009;19:4829–36.
[31] Wang Z-S, Koumura N, Cui Y, Takahashi M, Sekiguchi H, Mori A, et al. Hexylthiophene-functionalized carbazole dyes for efficient molecular photovoltaics: tuning of solar-cell performance by structural modification. Chem Mater 2008;20:3993–4003.
[32] Masuda N, Tanba S, Sugie A, Monguchi D, Koumura N, Hara K, et al. Stepwise construction of head-to-tail-type oligothiophenes via iterative palladium-catalyzed CH arylation and halogen exchange. Org Lett 2009;11:2297–300.
[33] Pavlishchunk VV, Addison AW. Conversion constants for redox potentials measured versus different reference electrodes in acetonitrile solutions at 25 °C. Inorg Chim Acta 2000;298:97–102.
[34] Clifford JN, Palomares E, Nazeeruddin MK, Grätzel M, Durrant JR. Dye dependent regeneration dynamics in dye sensitized nanocrystalline solar cells: evidence for the formation of a ruthenium bipyridyl cation/iodide intermediate. J Phys Chem C 2007;111:6561–7.
[35] Qin P, Yang X, Chen R, Sun L. Influence of π-conjugation units in organic dyes for dye-sensitized solar cells. J Phys Chem C 2007;111:1853–60.
[36] Uemura Y, Mori S, Hara K, Koumura N. Carbazole dyes with alkyl-functionalized thiophenes for dye-sensitized solar cells: relation between alkyl chain length and photovoltaic performance. Chem Lett 2011;40:872–3.
[37] Nakade S, Kanzaki T, Wada Y, Yanagida S. Stepped light-induced transient measurements of photocurrent and voltage in dye-sensitized solar cells: application for highly viscous electrolyte systems. Langmuir 2005;21:10803–7.
[38] Duffy NW, Peter LM, Rajapakse RMG, Wijayantha KGU. A novel charge extraction method for the study of electron transport and interfacial transfer in dye sensitised nanocrystalline solar cells. Electrochem Commun 2000;2:658–62.